JTTEE5 9:250-258
© ASM International

Peer Reviewed

Droplet Splashing during Arc Spraying of Steel and the Effect on Deposit Microstructure

A.P. Newbery and P.S. Grant

(Submitted 15 April 1999; in revised form 7 December 1999)

The mechanism by which droplet deposition occurs is important when filling substrate features for the electric arc spray forming of steel tooling. Particle image velocimetry and high-speed video imaging techniques have been used to observe droplet deposition, particularly with regard to the behavior of droplets originating from splashing. Droplet splashing on deposition has been seen to be significant, and splash droplets form a large proportion of the overspray. The splash droplets are smaller and, when first created, move slower than the parent droplet. When spraying into deep features, the lateral and upward movement of splash droplets acts as a mechanism for deposit formation onto surfaces in shadow from the main spray. Microstructural study has shown that oxidation of the splash droplets before redeposition leads to a deposit with a high fraction of oxide. Simultaneous growth of deposit formed directly from the spray, and from splash droplets, results in a banded microstructure containing elongated macropores. A mechanism for such microstructural evolution is proposed.

Keywords rapid production tooling, deep substrate features, spray diagnostics, droplet splashing, microstructural evolution

1. Introduction

In a wide variety of commercially important thermal spray processes, the manner in which sprayed droplets impinge, spread, and solidify on deposition is critical in influencing the subsequent properties of the manufactured coating or deposit. The first droplets to deposit will determine the properties at the coating-substrate interface, the most important consequence of which is the coating adhesion.[1,2] In the case of spray forming of freestanding shapes for mold tooling, the first droplets to deposit will determine the extent of replication[3] and tooling wear properties. As deposition continues, droplet deposition behavior controls the bulk microstructure, such as the volume fraction, morphology, and size of porosity,[4,5,6] consequently determining the coating bulk properties. At all stages of deposition, droplet rebounding or splashing leads to a reduction in process yield.[7] Subsequent incorporation of this initially rejected material by engulfment may lead to a degradation in coating properties. [4]

The droplet impact angle,[4,5] velocity, [8–11] diameter, [11] extent of solidification, temperature, [9,10] thermophysical properties, [11–15] and deposition surface roughness and temperature [11,15] all influence droplet deposition behavior during thermal spraying in a complex, inter-related manner. In order to understand further these phenomena, considerable effort has been expended in (a) measuring or modeling the state of the spray at impact with the deposition surface; and (b) measuring or modeling the subsequent deformation of the droplets. A number of analytical and time resolved models that describe droplet spreading over a smooth or roughened surface have been developed.[6,8,16–25] Most of these models or analytical expressions are in broad agreement and show that droplet deposition is a complicated process occurring over the scale of 10^{-6} to 10^{-3} s. Recently, three-dimensional modeling of droplet deposition has taken splashing into account and has shown splashing to be a significant phenomenon in deposition.[26] Experimental validation of droplet deposition models has largely used measurement of the shape of resulting droplet "splats" after solidification,[9,16,12–14] rather than by direct observation of deposition under realistic thermal spray conditions.

The development of high-speed video cameras combined with macrolenses has facilitated direct observation of droplet impact. However, imaging of droplet deposition has tended to use droplets of larger diameter and/or lower velocity than those typically found in thermal spraying techniques.[17,24,25,27,28] It is uncertain whether observation of deposition behavior, for example, of a 5 mm droplet with a velocity of 10 ms^{-1} is relevant to thermal spraying conditions where the droplets are typically 50 to 100 μm and impacting at velocities greater than 50 ms^{-1}.[8] The use of lasers for short interval illumination has enabled excellent video imaging of thermal sprays,[29] but at flame rates that are too slow to obtain a fully time-resolved sequence of a single droplet during impact.

In particle image velocimetry (PIV), a laser is used to illuminate a thin two-dimensional (2-D) light sheet within a particle flow domain. The laser is rapidly double pulsed to obtain two consecutive images separated by a short time interval in a synchronized camera. Computer software is then used to analyze the two digital images and identify particle pairs. Knowing the time interval between images and the position of particles in each image, a 2-D vector map of particle velocities is readily obtained. Particle image velocimetry has been used to investigate the flow of gases in combustion chambers, convection in water, flow of water jets, and flow around airfoils.[30] In these cases, the fluid was seeded with fine particles, and it was assumed that these particles move with the same velocity as the fluid, *i.e.*, seeded flow. In thermal sprays, where the droplets themselves are illuminated, PIV has been used to find the velocities of the droplets in flight.[31]

A. P. Newbery and **P. S. Grant,** Oxford Centre for Advanced Materials and Composites, Department of Materials, University of Oxford, Oxford OX1 3PH, United Kingdom.

This paper gives a preliminary report of the use of PIV for the investigation of the behavior of droplets close to the substrate, including impact. These results are correlated with high-speed video camera images of droplet deposition during spraying. The main thrust of the paper is to relate droplet deposition behavior to complex microstructural features in steel tooling manufactured by electric arc spraying onto shaped substrates. The spray forming process is excellent at reproducing fine detail, but problems arise when trying to fill deep substrate features, such as a notch. In general, poor quality deposit is formed on the notch sidewalls, and the deposit at the entrance to the notch can close together before the notch is filled completely. This latter effect is known as bridging. A current rule-of-thumb is that nothing deeper than a square sectioned notch can be filled satisfactorily. However, the limitations of the process are subjective. For example, very large square notches can be filled, but shallower features can also exhibit problems. Knowledge about droplet deposition behavior, and its effect on microstructure, will enable improvements to be made to the quality of the deposit in deep features and extend the range of tooling shapes that can be produced without the need for post-spray machining. More generic implications of droplet deposition behavior in thermal spray processes are also discussed.

2. Experimental Procedure

2.1 PIV and High-Speed Imaging

The experimental setup for PIV investigation in the current study is shown schematically in Fig. 1. A Quantel Twins (Quantel, Les Ulis Cedex, Paris) Nd:YAG 532 nm 2×150 mJ laser system was used to create a light sheet parallel to, and passing through, the spray axis. A TSI (TSI Inc., St. Paul, MN) cross correlation CCD camera viewed the illuminated spray normal to the light sheet and the spray axis. A 1 nm width, 532 nm band pass filter was used to remove most of the arc light and light emitted from the hot steel droplets. The laser pulses and the CCD camera shutter were synchronized using a TSI LaserPulse computer controlled synchronizer. The detail of the timing of the laser pulse with the camera shutter is shown schematically in Fig. 2. Double image pairs were taken at a rate of 15 Hz with an interval of 7 μs between the images within the same pair. The digitized-PIV images were analyzed using TSI INSIGHT software to generate a series of 15 vector maps, which were then combined to obtain a time-averaged velocity vector map.

A Kodak (Eastman Kodak Co., Rochester, NY) HS4540 digital video camera was used to obtain sequences of images of steel droplet deposition at a frame rate of 40,000 Hz during spraying, so that each image was exposed for 25 μs (1/40,000th s). At this frame rate, the images were composed of an array of 64×64 pixels. The video camera was placed level with the substrate surface, in the same position as the CCD camera in the PIV experiments. The spray droplets were imaged by their natural emitted radiation and no external illumination was used.

2.2 Spraying

For the PIV and high-speed imaging experiments, a Sulzer Metco SmartArc (Sulzer Metco (US) Inc., Westbury, NY) electric arc spray system was used to spray 0.8% C steel wire (TAFA 38T) with N_2 atomizing gas. The arc current was 150 A, the arc voltage was 28 V, and the N_2 pressure was 0.2 MPa. The arc gun was fixed to a sealed chamber with an extraction system and with appropriate optical access for PIV and imaging. For the PIV experiments, a rotating 50 mm o.d. cylindrical mild steel substrate was used. For the high-speed imaging experiments, a rectangular 10 mm thick steel plate positioned normal to the spray axis was used as the substrate. The plate contained a 10 mm square notch, located on the spray axis. A square notch, as mentioned previously, is at the current limit of the spray forming process for producing satisfactory deposit filling of features. For both PIV and high-speed imaging experiments, the substrates were placed at an axial distance of 160 mm from the arc region.

Steel deposits were also sprayed using a robotic spray system developed for the electric arc spray forming of hard tooling.[32] In this case, a TAFA 8090 (TAFA, Concord, NH) electric arc spray system was used to spray 0.8% C steel wire, with the gun attached to a KUKA (KUKA, Augsberg, Germany) robot. Al-

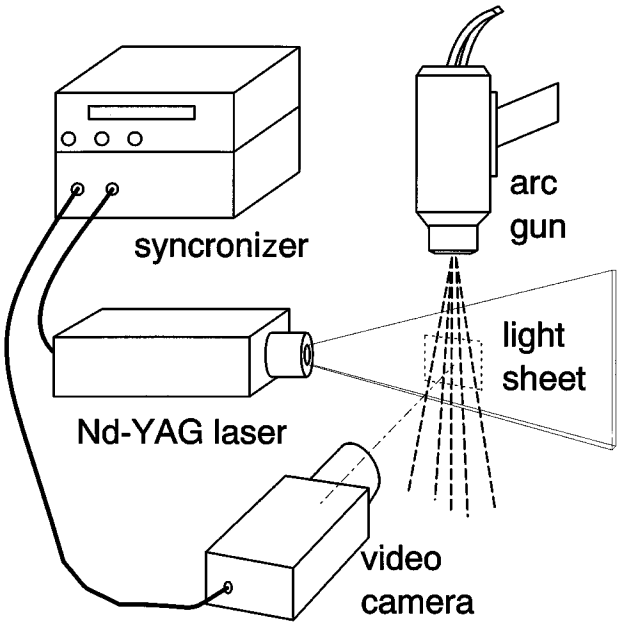

Fig. 1 Schematic diagram showing the experimental arrangement for the use of PIV to look at the droplet flow when electric spraying (chamber and substrate not shown)

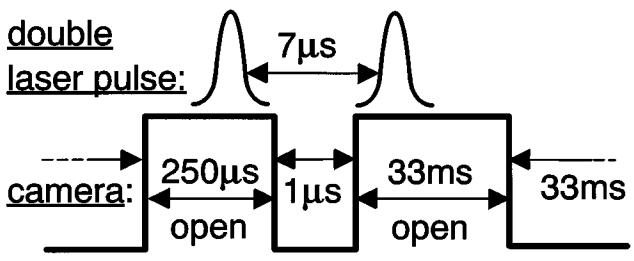

Fig. 2 Schematic diagram showing how the two laser pulses were timed and synchronized with the video camera to produce a PIV image pair of the spray droplets

though N_2 atomizing gas was again used, spraying was performed in an air filled spray booth. A flat, 200 × 150 mm, alumina based, freeze cast ceramic rectangular substrate, containing a 40 × 20 mm (width × depth) rectangular cross-sectional notch, was placed on a rotating table at an axial distance of 160 mm from the arc region. The sidewalls of the notch had a 2° taper to facilitate removal of the ceramic freeze east from the original template. During spraying, the gun, orientated at 90° to the substrate, was traversed parallel to the substrate at a constant height, to form a deposit of ~10 mm uniform thickness.

In summary, PIV and high-speed imaging experiments were performed using a sealed chamber, which allowed close, convenient, and protected location for the diagnostics equipment, whereas experiments to generate realistic microstructures during the manufacture of sprayed steel tooling were performed with a customized robotic system. The presence of a notch, similar in size and shape to the current limitations of the process, would highlight the microstructural problems caused by spraying into deep features.

2.3 Microscopy and Image Analysis

The steel deposit formed by the robotic spray system was sectioned through thickness perpendicular to the length of the notch and polished using standard metallographic techniques. Macroporosity was observed and sketched using the naked eye. An Olympus (Olympus Optical Co., Ltd., Tokyo, Japan) BH optical microscope was used for examination of the microstructure in the unetched condition. The vernier x-y scale of the microscope translation table was used to map the deposit cross-sectional free-surface profile on a 0.5 mm square grid, with an accuracy of 0.1 mm.

A Buehler Omnimet (Buehler, Lake Bluff, IL) image analysis system was used to quantify the area fraction of deposit steel (white), oxide (dark gray), and porosity (black). The technique of image analysis is subject to large systematic errors and so it is unlikely to yield true values of porosity. However, for given illumination conditions, each measurement has only a small error (about ±0.1% porosity). Image analysis is thus suitable for accurate comparative statements about porosity, even when the mount of porosity measured is quite low.

3. Results

Figure 3 shows a PIV vector map for an arc spray near a 50 mm diameter cylindrical substrate rotating at 36 rpm. The overall flow of droplets was from the arc region toward the substrate. The droplet velocity vectors were generally parallel to the spray axis, with a maximum velocity located close to the spray axis. It is evident from Fig. 3 that the spray axis, where the vectors are largest, was not aligned with the center of the cylinder. Figure 3 also shows that near the surface of the substrate at the spray axis, the velocity vectors were reversed, with droplets having a negative velocity (in the current convention) and a relatively low magnitude of velocity. Away from the spray axis, Fig. 3 shows these droplets were entrained within the main flow of the spray, progressively accelerated, and finally swept around the substrate to be removed as overspray. The reverse droplet flow near the substrate surface is emphasized by Figure 4,

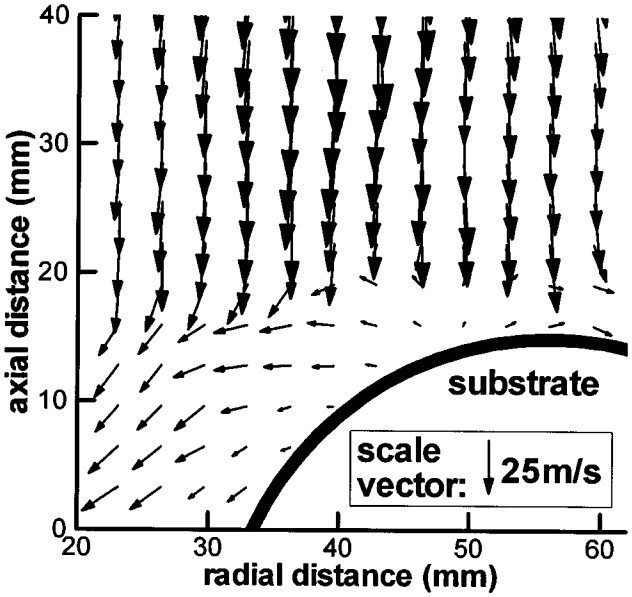

Fig. 3 PIV vector map showing the 2-D distribution of time-averaged droplet velocities when electric arc spraying steel onto a cylindrical substrate. The vector lengths, and arrowhead sizes, are proportional to velocity, and so a scaling vector is given for reference.

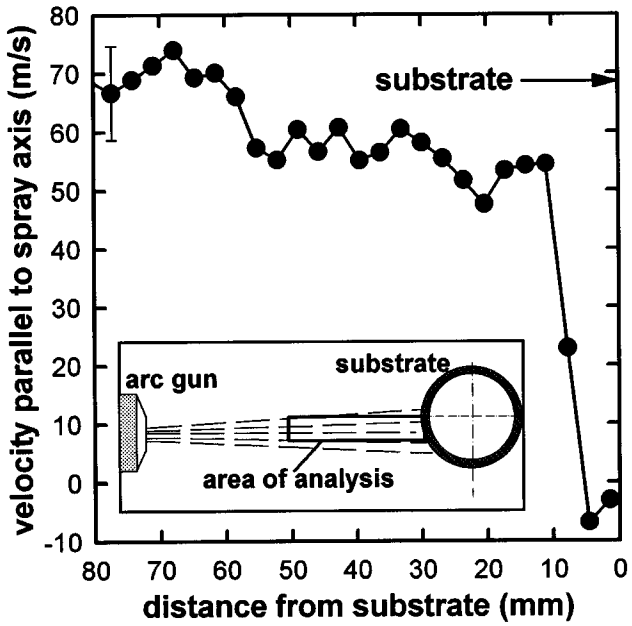

Fig. 4 Graph showing the variation in the axial component of the average droplet velocity (measured by PIV) near the spray axis when electric arc spraying steel onto a cylindrical substrate of 50 mm O.D. The schematic diagram insert shows the area in the spray used to select the PIV data, the averaged values of which are plotted in the graph.

which shows the axial component of velocity for those droplets that traveled close to the spray axis, as a function of axial distance away from the substrate. Droplet velocities decreased steadily with decreasing distance from the substrate (increasing axial distance), from ~70 ms^{-1} at 80 mm from the substrate to ~50 ms^{-1} at 20 mm from the substrate. At a distance of ~10 mm

from the substrate surface, the flow of droplets abruptly became negative, with a magnitude of 5 to 10 ms^{-1}

In general, high-speed imaging of droplet deposition showed that the majority of droplets underwent extensive splashing on impact and that a significant proportion of material was rejected from the substrate in the form of splash droplets. The exact number of splash droplets generated per impact was difficult to count but, in general, appeared to be in the range of 10 to 20. At low magnifications and video speeds, a haze of splash droplets, close to the substrate surface, was continuously present during spraying.

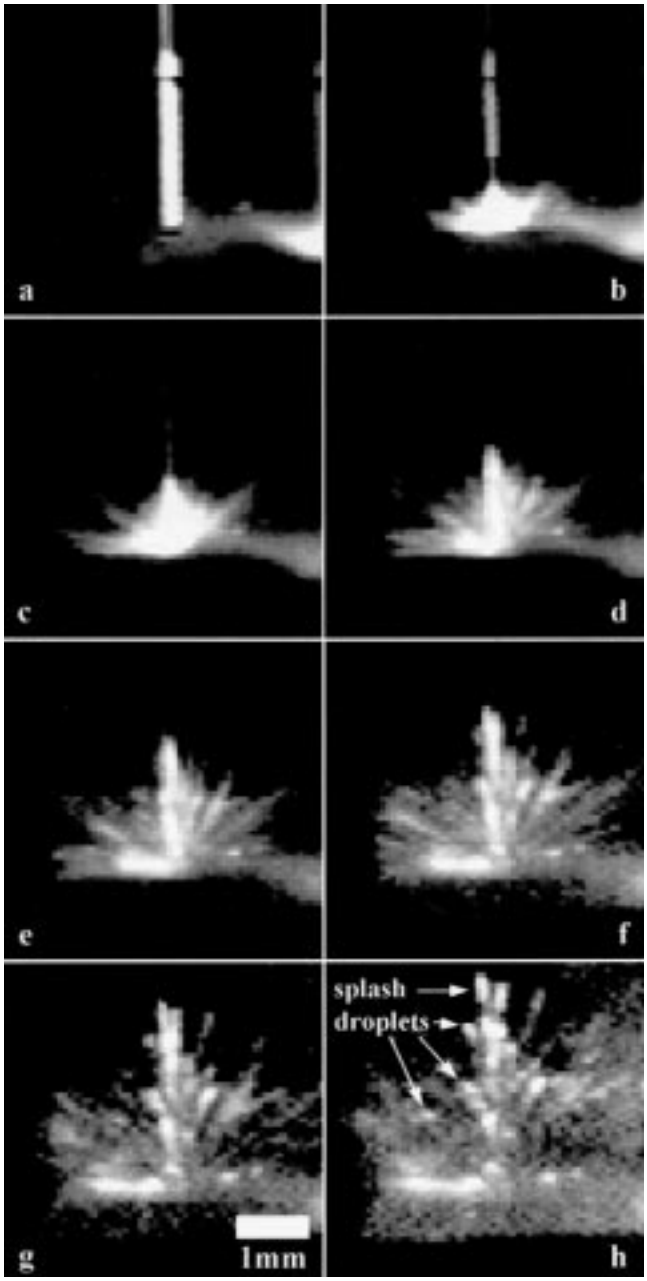

Fig. 5 (a) through (h) Sequence of video images obtained at 40,000 frames per second, showing the splashing of an electric are spray steel droplet upon impact with the substrate

Figure 5 shows a sequence of images for a droplet impacting at ~90 ms^{-1} onto the base of a notch in a stationary substrate. The incoming droplet appeared elongated due to its high velocity relative to the exposure time for the image. Some blurring also occurred because of the high intensity of the natural emitted radiation from the droplet. Consequently, the droplet size was difficult to measure accurately. Figure 5 shows that, on impact, the droplet splashed and about a dozen smaller, slower moving droplets were thrown upward, away from the substrate, at a range of angles. The velocity of the splash droplets was difficult to measure accurately, because motion was not necessarily in the plane of the image but was estimated at ~20 ms^{-1}. The diameters of the splash droplets were also difficult to measure because they were close to the pixel resolution of the camera.

Figure 6 shows the cross-sectional profile of a robot sprayed deposit, near the sidewall of a 40 × 20 mm rectangular section notch, superimposed with sketched macroporosity. The positions

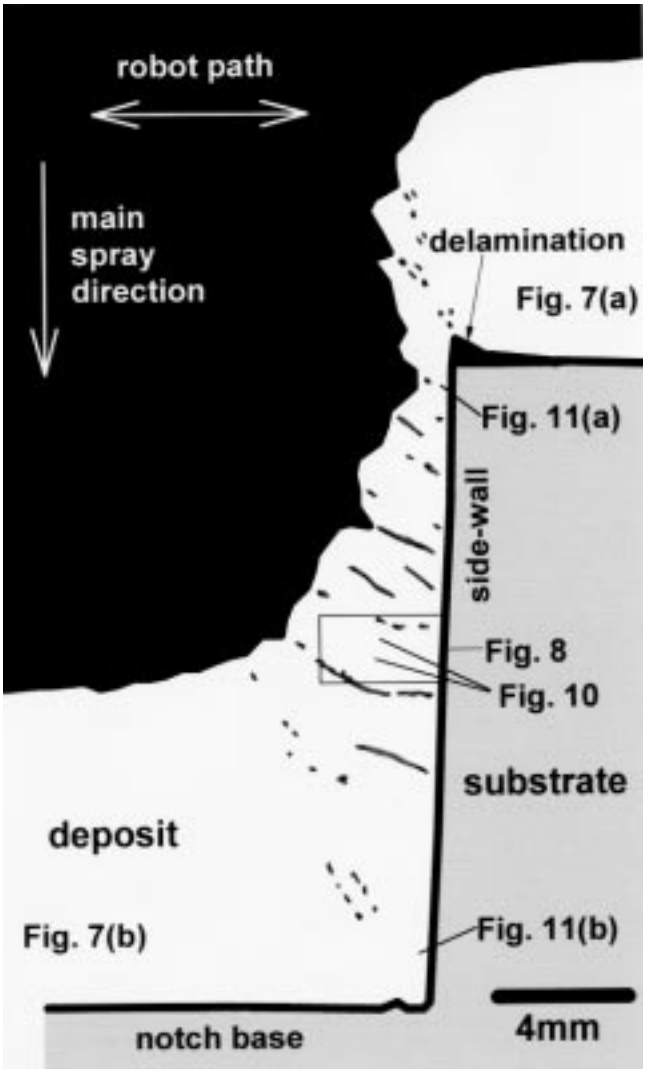

Fig. 6 Diagram showing the profile (graphically plotted) and macroporosity (sketched) of a steel deposit formed by electric are spraying onto a ceramic substrate containing a 40 × 20 mm notch (right-hand part only). Positions of the optical micrographs in Figs. 7, 8, 10, and 11 are indicated.

of the micrographs in Figs. 7, 8, 10, and 11 are labeled in Fig. 6. The deposit microstructure away from the notch, shown in Fig. 7(a), was typical of arc sprayed steel, consisting of steel splats, iron oxide, and pores. However, the oxide and porosity area fractions of ~10 and 4%, respectively, for the deposit in the notch base, shown in Fig. 7(b), were greater than the values of ~7.5 and 2.5% in the deposit away from the notch. The number of presolidified droplets (PSDs) for the deposit in the notch base was about double that for the deposit away from the notch. In both cases, the smaller PSDs, of about 10 μm in diameter, were usually surrounded by oxide.

Figure 8 shows the overall deposit microstructure near the notch sidewall, and Fig. 9 shows a schematic diagram of the microstructure. The deposit near the sidewall had a comparatively rough surface, as shown previously in Fig. 6. Linear arrangements of macropores propagated up and away from the sidewall at an angle of ~65°, as shown in Fig. 8 and 9. The macropores were often elongated up to 2 mm. In general, the macroporosity emerged at the troughs of the rough surface. The line of macropores closest to the notch base defined the boundary between deposit originating from the sidewall and that from the notch base. The sidewall deposit microstructure was composed of bands of two different types of material (type 1 and type 2), as shown in Fig. 8 and 9, parallel to the lines of macropores, in the order type 1, macropores, type 2, type 1, macropores, etc.

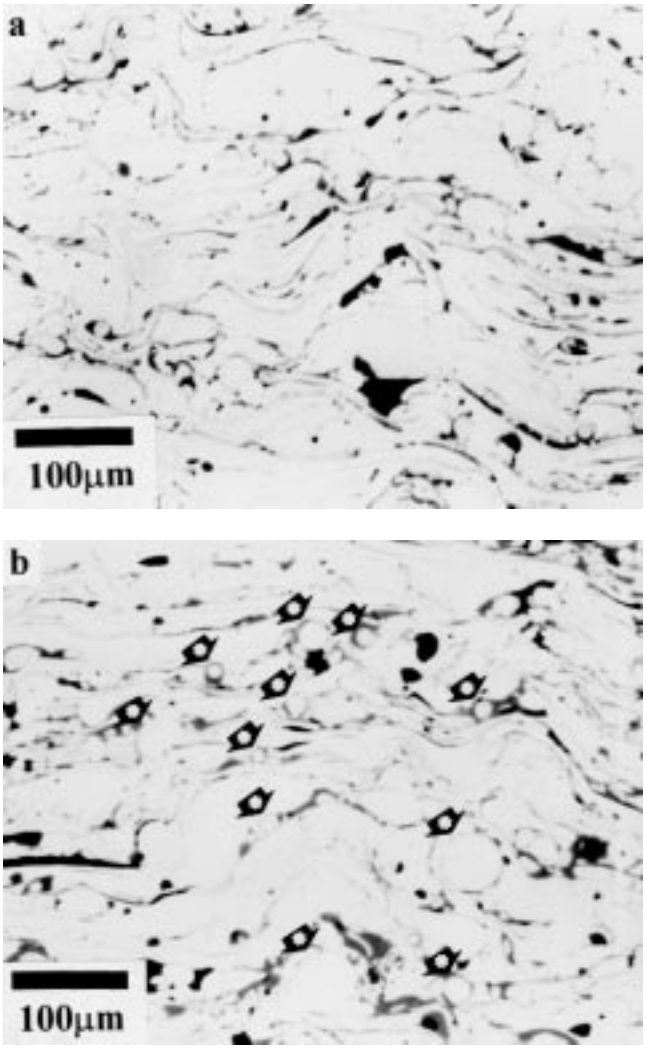

Fig. 7 Optical micrographs showing the typical microstructures of a steel deposit formed by electric arc spraying onto a ceramic substrate containing a 40 × 20 mm notch: (a) away from the notch and (b) near the notch base. Some of the PSDs in (b) are indicated with arrows. The positions of these micrographs are shown in Fig. 6.

Type 1: On the upper side of the macropores, there were bands containing ~20% oxide, and porosity varying locally from ~3 to ~20%, as shown in Fig. 8, 9, and 10(b). These high oxide bands contained a very high number of PSDs. The diameters of the PSDs were in the range 5 to 40 μm. For most cases, as shown in Fig. 10(b), the PSDs were embedded in an oxide matrix. The average steel splat length was ~50 μm compared with ~200 μm splat length in the notch base, or away from the notch. The splats were orientated between 0° and ~45° from the sidewall.

The deposit material very close to the notch sidewall was type 1. The average area fraction of oxide and porosity (and number of PSDs) increased from the bottom to the top of the notch, from ~13% oxide and ~8% porosity near the notch base comer (Fig. 11b) to ~28% oxide and ~13% porosity near the notch top corner (Fig. 11a). The region near the notch top corner was mechanically very weak and susceptible to cracking.

Type 2: On the lower side of the macropores were bands of comparatively higher quality, as shown in Fig. 8, 9 and 10(a), similar to deposit formed away from the notch. The oxide and porosity area fractions were as low as ~8% and ~2.5%, respectively. The splats were orientated at ~60° from the sidewall. Local values of oxide were increased by the presence of linear arrays of PSDs, surrounded by oxide, roughly perpendicular to the splat structure, as shown in Fig. 10(a).

4. Discussion

High-speed imaging of droplet deposition has shown that significant droplet splashing occurs on deposition. A proportion of impacting droplets subdivides into smaller, slower moving droplets, which move upward and sideways away from the substrate surface. The PIV measurements have confirmed that there is a significant negative flux of particulate material near the substrate surface. In the PIV measurements, the number of droplets generated by splashing events is large enough to mask the lower number of impacting droplets, because the INSIGHT PIV software assigns the mode of the local velocity distribution within a particular spatial measurement volume, not an average or mean of the distribution. The PIV measurements and imaging estimates of incoming droplet velocities are in broad agreement at 50 to 90 ms^{-1}. Similarly, both techniques indicate velocities of 5 to 20 ms^{-1} for droplets generated during splashing. Improvements in the high-speed imaging may be realized by reducing the exposure time for each image and by using external laser illumination instead of natural radiation emitted by the droplets, similar to the LaserStrobe [29] approach. Image blurring will be removed and the bias toward larger, brighter droplets will also be reduced.

On the basis of the high-speed imaging, PIV, and microstructural characterization, the following mechanism for deposit

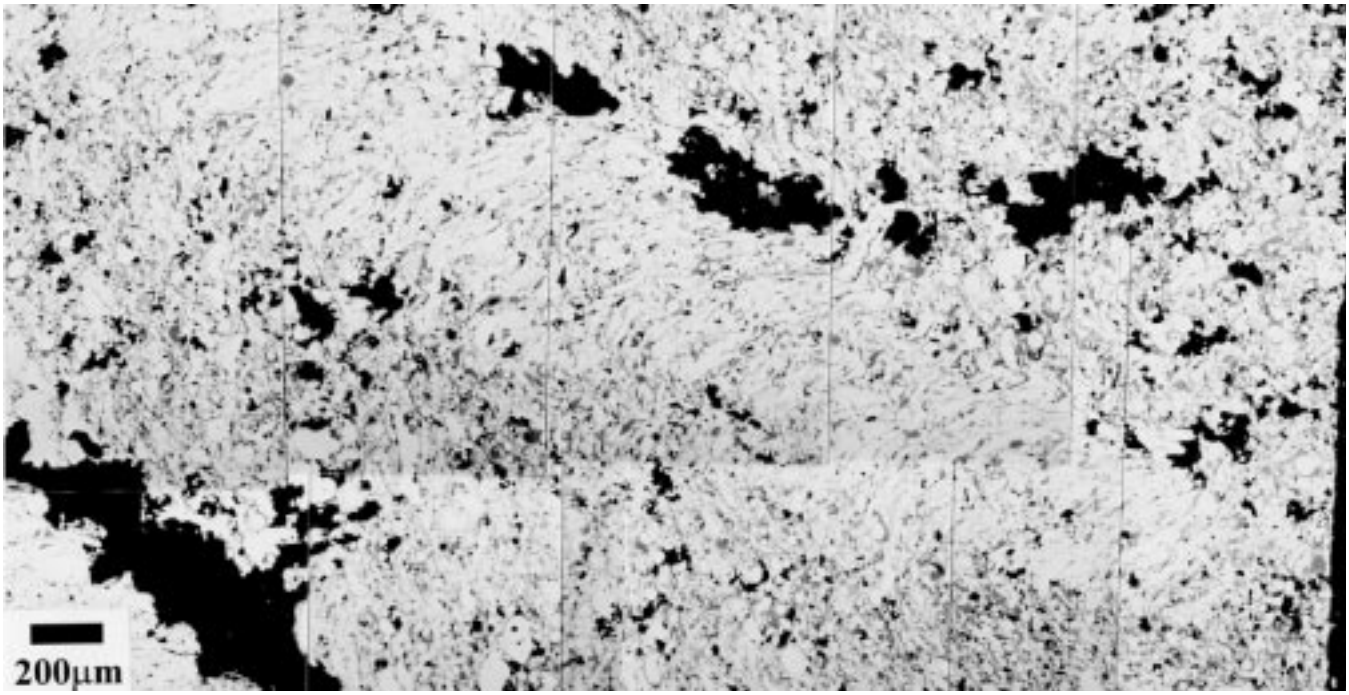

Fig. 8 Composite optical micrograph showing the microstructure near the notch sidewall of a steel deposit formed by electric arc spraying onto a ceramic substrate containing a 40 × 20 mm notch. The position of this micrograph is shown in Fig. 6.

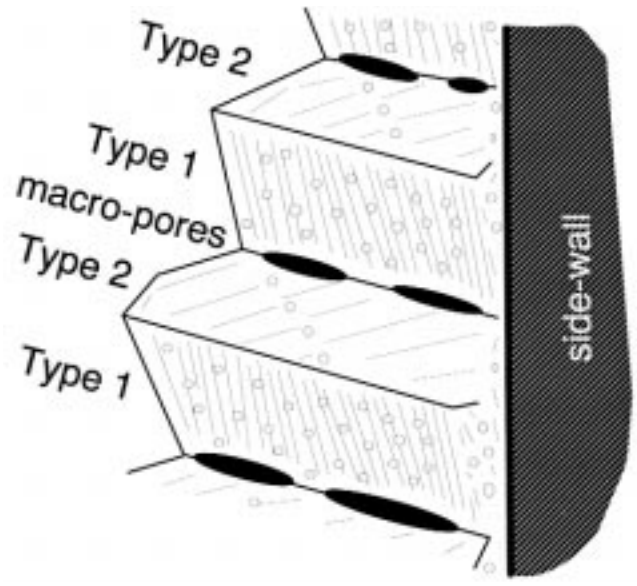

Fig. 9 Schematic diagram showing the typical microstructure near the sidewall of a steel deposit formed by electric arc spraying onto a ceramic substrate containing a 40 × 20 mm notch

formation on the notch sidewall is proposed, as shown schematically in Fig. 12.

Stage I: The droplets in the main spray impact on the notch base splash and generate a large number of rapidly cooling, slower moving, smaller droplets. Because of the large increase in liquid surface area on splashing, and their relatively slow velocity, significant oxidation of the splash droplets occurs; *i.e.*, $2Fe + O_2 \rightarrow 2FeO$. FeO and Fe-0.8% C have liquidus temperatures of 1371 to 1424 °C [33] and 1470 to 1530 °C (depending on carbon loss during spraying), [34] respectively. Therefore, splash droplets may consist of a solid steel center surrounded by a molten oxide exterior. Because of the acute angle between the spray axis and the notch side-wall, little of the main spray hits the sidewall directly.

Stage II: Upward and lateral trajectories of splash droplets intersect the notch sidewall and secondary deposition occurs. If the splash droplets have partially solidified, then PSDs in an oxide matrix are formed. If the droplets are still fully liquid, then they deposit conventionally. The precise extent of solidification and oxidation will depend on the splash droplet thermal history prior to secondary deposition. Sidewall deposit near the notch base has a lower PSD and oxide content than sidewall deposit at the notch top because splash droplets have longer flight times to the notch top and, consequently, increased solidification and oxidation prior to secondary deposition. Because of the mixture of PSDs and oxide, and the non-normal angle of secondary deposition, the initial sidewall deposit has a rough perturbed surface.[35]

Some splash droplets have the necessary trajectories and sufficient momentum to escape from the notch entirely. These are then entrained into spray gas flow moving over the deposit surface and are removed as "overspray." Some splash droplets fall back into the notch, secondary deposition occurs along with primary deposition on the notch base, and there is a consequent increase in oxide and porosity.

Stage III: Primary deposition of droplets from the main spray on sections of the perturbed surface that are now at an angle closer to 90° to the main spray axis and this forms relatively good quality deposit (type 2). Secondary deposition of smaller, oxidized droplets from splashing on sections of the perturbed surface that

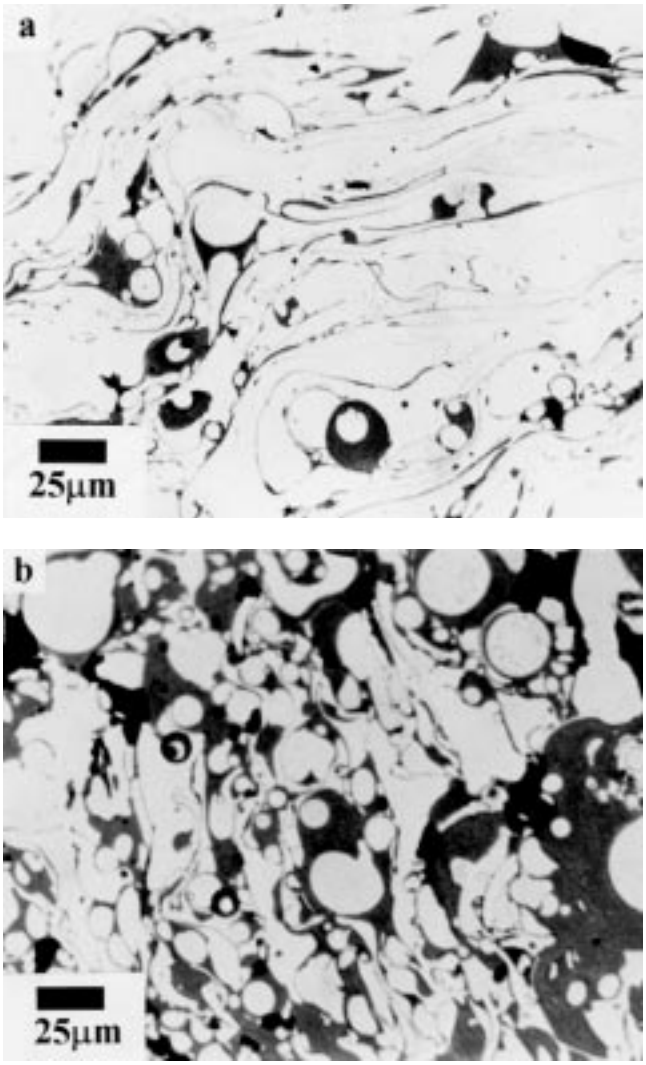

Fig. 10 Optical micrographs showing the different types of structure near the notch sidewall of a steel deposit formed by electric arc spraying onto a ceramic substrate containing a 40 × 20 mm notch: (a) type 2 and (b) type 1. The positions of these micrographs are shown in Fig. 6.

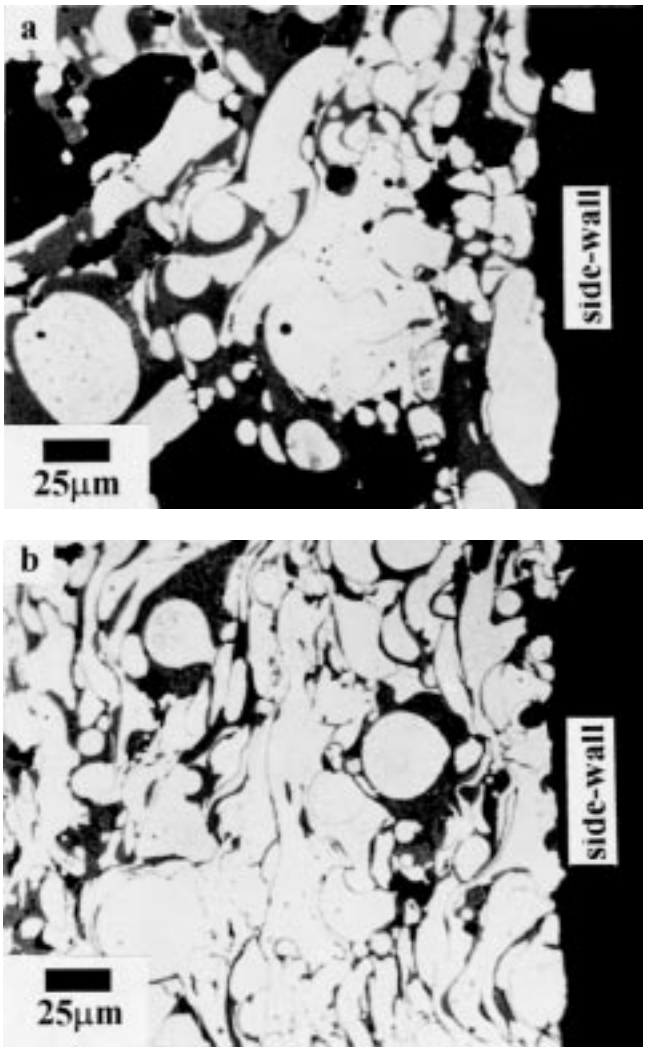

Fig. 11 Optical micrographs showing the structure at the notch sidewall of a steel deposit formed by electric arc spraying onto a ceramic substrate containing a 40 × 20 mm notch: (a) near the notch top comer and (b) near the notch base. The positions of these micrographs are shown in Fig. 6.

are preferentially orientated toward the point of splashing forms relatively porous, high oxide material (type 1). The simultaneous primary and secondary deposition enables the perturbations to grow away from the sidewall. Lines of elongated macropores form at the boundaries between adjacent perturbations.

As described above, droplet splashing is an important mechanism to allow continued deposit formation on parts of the substrate either in shadow or at an acute angle from the main spray. However, under the experimental conditions considered in this paper, the deposit formed this way is of low quality because of the oxidation of the splash droplets prior to redeposition. In addition, it is not clear if splashing is generally a beneficial mechanism for the filling of deep substrate features, since the evidence suggests that splashing is the major cause of bridging. A change in the spraying conditions to increase the amount of splashing may improve the initial amount, and quality, of deposit on the sidewall but will probably be counterproductive in that it promotes earlier bridging.

For the range of real shapes produced by spraying for tooling applications, there will be cases where it is impossible to spray directly onto one or more of the substrate surfaces, and splashing may be the only way of filling certain features. Spraying in an inert atmosphere may improve the quality of splashed material by reducing oxidation, but may reduce the amount of splashing itself, as incoming droplets will have a lower superheat. Even if the amount of splashing is increased and the extent of oxidation is decreased, the lines of macropores are probably unavoidable to some extent, as they are fundamental to the geometry of primary and secondary deposition. Such microstructural features will leave a deposit that is vulnerable to fracture.

These preliminary results focus on the splashing, redeposition, microstructure, and shape evolution during thermal spraying under model conditions. However, the relative motion between the spray(s), the substrate, and the angle of impact, i.e., the path plan, and the droplet characteristics such as velocity and size distribution must be optimized in order to replicate complex

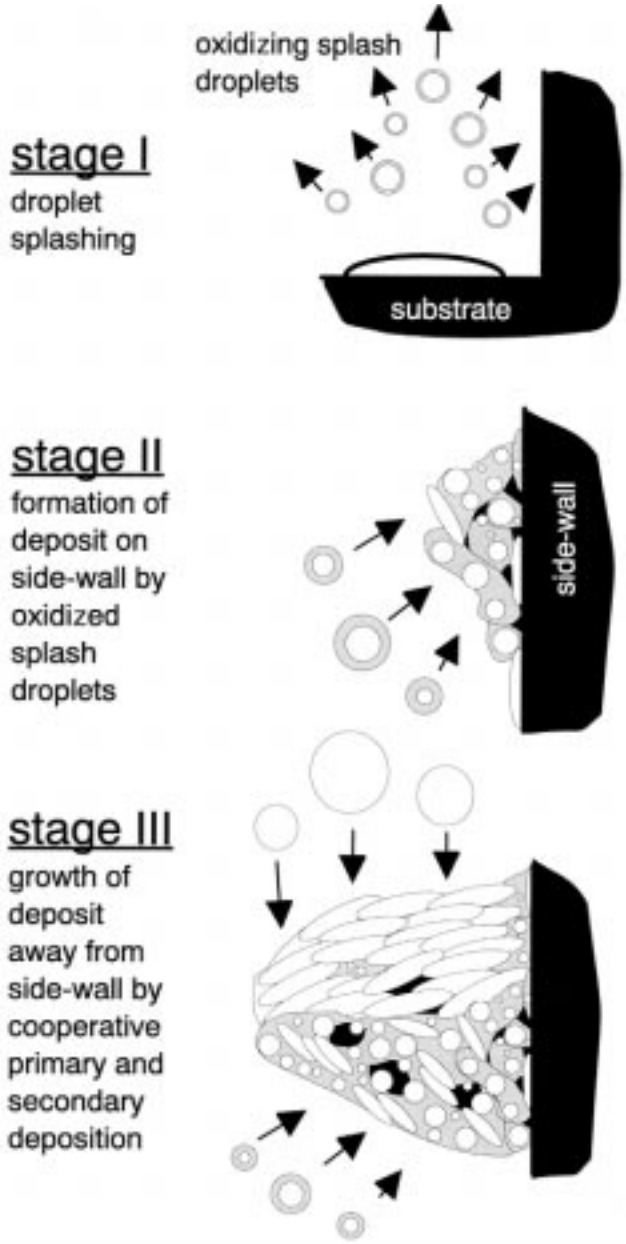

Fig. 12 Schematic diagram of the mechanism whereby splashing of droplets on primary deposition, followed by cooperative primary and secondary deposition, leads to a banded type 1/type 2 microstructure near the sidewall of a notch.

geometry with good quality sprayed material. The PIV and improved high-speed imaging measurements are currently being combined with numerical simulations to produce a model of the transient buildup of complex shapes during spraying. Work is also being carried out to investigate the effect of substrate feature size and shape, the end objective being to optimize the process with regard to filling and to produce a rule book on what tooling features can, or cannot, be sprayed satisfactorily. It is clear from the results presented here that feature depth is important. A deeper notch, with the same size aperture, will have greater amounts of splashed material and oxide on the sidewall, and bridging is more likely to occur, before the notch is filled with deposit.

The manufacture of sprayed tooling is a relatively specialized thermal spray application, but understanding of droplet splashing phenomena has more generic implications. In the majority of thermal spray applications, the spray is projected at ~90° onto a substrate that does not contain deep features. Most of the small splash droplets are then swept away by the lateral flow of the gas and usually have little obvious effect on coating microstructure. This is consistent with overspray particle size distributions, which have a smaller mean particle size than those collected from the full spray.[36] Therefore, it is possible to suggest that the yield and deposition efficiency of spraying may be increased by manipulation of deposition behavior to reduce droplet splashing.

There are spraying applications, aside from the manufacture of rapid tooling, where splash droplets are important in coating formation, for example, when building up a thick coating in one pass and the gun traverse speed is too slow. Splashing is then a primary cause of high roughness, porosity, and oxide. Also, when spraying is carried out at angles less than 90°, for the coating of cylinder bores, the splash droplets become integrated into the coating and form a significant part of the microstructure.[4,35] In both of these cases, the coating quality is a direct function of splashing and the optimum spraying conditions may be achieved by taking this into consideration.

5. Conclusions

Particle image velocimetry and high-speed video imaging have been used to observe droplet deposition during electric arc spraying, particularly with regard to the behavior of droplets originating from splashing. Droplet splashing on deposition has been found to be significant during the electric arc spraying of steel, and splash droplets form a large proportion of the overspray. When spraying into deep features for tooling applications, the lateral and upward movement of splash droplets acts as a mechanism for deposit formation onto those surfaces in the shadow from the main spray. However, excessive oxidation of the splash droplets before re-deposition leads to a deposit with a high fraction of oxide. Simultaneous growth of the deposit formed directly from the main spray and from splashing results in a banded microstructure containing elongated macropores.

Acknowledgments

The authors thank the United Kingdom Engineering and Physical Sciences Research Council (Grant No. GR/L30954), Sprayform Holdings Ltd. (SHL (Ford), Dearborn, MI), and the Royal Society for financial support; Allen Roche of SHL for assistance with the robotic spraying; Sy Mangat, Kodak Ltd. (Hemel Hempstead, United Kingdom), for help with the high speed video imaging measurements; and Martin Hyde, Bristol Industrial and Research Associates Ltd. (BIRAL, Portishead, United Kingdom), and Helmut Kronewetter, TSI GmbH (TSI, Aachen, Germany), for advice on the PIV measurements.

References

1. D.T. Gawne, B.J. Griffiths, and G. Dong: *Thermal Spraying—Current Status and Future Trends,* High Temperature Society of Japan, Japan, 1995, pp. 779-84.

2. V.V. Sobolev, J.M. Guilemany, J. Nutting, and J.R. Miquel: *Int. Mater. Rev.* 1997, vol. 42 (3), pp. 117-36.
3. K.A. Gross and A Kovalevskis: *J. Thermal Spray Technol.,* 1996, vol. 5 (4), pp. 469-75.
4. M.F. Smith, R.A. Neiser, and R.C. Dykhuizen: in *Thermal Spray Industrial Applications,* C.C. Berndt and S. Sampath, eds., ASM International, Materials Park, OH, pp. 603-08.
5. G. Montavon, C. Coddett, S. Sampath, H. Herman, and C.C. Berndt: in *Thermal Spray Industrial Applications,* C.C. Berndt and S. Sampath, eds., ASM International, Materials Park, OH, pp. 469-75.
6. H. Fukanuma: in *Thermal Spray: International Advances in Coating Technology,* C.C. Berndt, ed., ASM International, Materials Park, OH, 1992, pp. 767-72.
7. C. Kramer, V. Uhlenwinkel, and K. Bauckhage: *Solidification 1998,* S.P. Marsh, J.A. Dantzig, R. Trivedi, W. Hofmeister, M.G. Chu, E.J. Lavernia, and J.-H. Chun, eds., TMS, 1998, pp. 401-13.
8. R.C. Dykhuizen: *J. Thermal Spray Technol.,* 1994, vol. 3 (4), pp. 351-61.
9. C.J. Li, A. Ohmori, and Y. Harada: *Thermal Spraying—Current Status and Future Trends,* High Temperature Society of Japan, Japan, 1995, pp. 333-39.
10. S. Fantassi, M. Vardelle, P. Fauchais, and C. Moreau: in *Thermal Spray: International Advances in Coating Technology,* C.C. Berndt, ed., ASM International, Materials Park, OH, 1992, pp. 755-60.
11. M. Vardelle, A. Vardelle, A.C. Leger, and P. Fauchais: in *Thermal Spray Industrial Applications,* C.C. Berndt and S. Sampath, eds., ASM International, Materials Park, OH, 1994, pp. 555-62.
12. M. Fukumoto, S. Katoh, and I Okane: *Thermal Spraying—Current Status and Future Trends,* High Temperature Society of Japan, Japan, 1995, pp. 353-58.
13. X. Jiang and S. Sampath: *Solidification 1998,* S.P. Marsh, J.A. Dantzig, R. Trivedi, W. Hofmeister, M.G. Chu, E.J. Lavernia, and J.-H. Chun, eds., TMS, Warrendale, PA, 1998, pp. 439-48.
14. G. Montavon, S. Sampath, C.C. Berndt, H. Herman, and C. Coddet: *Thermal Spraying—Current Status and Future Trends,* High Temperature Society of Japan, Japan, 1995, pp. 365-69.
15. C. Moreau, P. Cielo, and M. Lamontagne: *Thermal Spray: International Advances in Coating Technology,* C.C. Berndt, ed., ASM International, Materials Park, OH, 1992, pp. 761-66.
16. J. Madejski: *Int. J. Heat Transfer,* 1976, vol. 19, pp. 1009-13.
17. G. Trapaga, E.F. Matthys, J.J. Valencia, and J. Szekely: *Metall. Trans. B,* 1992, vol. 23B, pp. 701-18.
18. H. Liu, E.J. Lavernia, and R.H. Rangel: *J. Phys. D: Appl. Phys.,* 1993, vol. 26, pp. 1900-08.
19. C. San Marchi, H. Lui, E.J. Lavernia, R.H. Rangel, A. Sickinger, and E. Muehlberger: *J. Mater. Sci.,* 1993, vol. 28, pp. 3313-21.
20. H. Fukanuma and A. Ohmori: in *Thermal Spray Industrial Applications,* C.C. Berndt and S. Sampath, eds., ASM International, Materials Park, OH, 1994, pp. 563-68.
21. H. Liu, E.J. Lavernia, and R.H. Rangel: *Acta Metall.,* 1995, vol. 43 (5), pp. 2053-72.
22. G. Montavon and C. Coddet: in *Thermal Spray Science and Technology,* C.C. Berndt and S. Sampath, eds., ASM International, Materials Park, OH, 1995, pp. 225-30.
23. J.-P. Delplanque and R.H. Rangel: *J. Mater. Sci., 1997,* vol. 32, pp. 1519-30.
24. V. Prasad, H. Zhang, and S. Sampath: in *Thermal Spray: A United Forum for Scientific and Technological Advances,* C.C. Berndt, ed., ASM International, Materials Park, OH, 1997, pp. 645-52.
25. J. Fukai, H. Asami, and O. Miyatake: *Solidification 1998,* S.P. Marsh, J.A. Dantzig, R. Trivedi, W. Hofmeister, M.G. Chu, E.J. Lavernia, and J.-H. Chun, ed., TMS, Warrendale, PA, 1998, pp. 473-83.
26. M. Bussmann, S.D. Aziz, S. Chandra, and J. Mostaghimi: in *Thermal Spray: Meeting the Challenges of the 21st Century,* C. Coddet ed., ASM International, Materials Park, OH, pp. 413-18.
27. D.M. Matson, M. Rolland, and M.C. Flemings: *Solidification 1998,* S.P. Marsh, J.A. Dantzig, R. Trivedi, W. Hofmeister, M.G. Chu, E.J. Lavernia, and J.-H. Chun, eds., TMS, Warrendale, PA, 1998, pp. 389-400.
28. W. Hofmeister, R.J. Bayuzick, G. Trapaga, D.M. Matson, and M.C. Flemings: *Solidification 1998,* S.P. Marsh, J.A. Dantzig, R. Trivedi, W. Hofmeister, M.G. Chu, E.J. Lavernia, and J.-H. Chun, eds., TMS, Warrendale, PA, 1998, pp. 375-87.
29. T.T. Hoffman: *Adv. Mater. Processes,* 1991, pp. vol. 140 (3), pp. 37-43.
30. H. Kronewetter: Unpublished paper for a Seminar on Flow Measurements, Tampere, Finland, 1995, available from TSI GmbH, Aachen, Germany.
31. R. Knight, R.W. Smith, Z. Xiao, and T.T. Hoffman: in *Thermal Spray Industrial Applications,* C.C. Berndt and S. Sampath, eds., ASM International, Materials Park, OH, 1994, pp. 331-36.
32. A.P. Newbery, P.S. Grant, R.M. Jordan, A.D. Roche, and T. Carr: in *Thermal Spray: Meeting the Challenges of the 21st Century,* C. Coddet, ed., ASM International, Materials Park, OH, 1998, pp. 1223-28.
33. H.A Wriedt: in *Binary Alloy Phase Diagrams,* T.B. Massalski, ed., ASM International, Materials Park, OH, 1990, pp. 1739-44.
34. H. Okamoto: in *Binary Alloy Phase Diagrams,* T.B. Massalski, ed., ASM International, Materials Park, OH, 1990, pp. 842-48.
35. M.P. Kanouff, R.A. Neiser, and T.J. Roemer: *J. Thermal Spray Technol.,* 1998, vol. 7 (4), pp. 219-28.
36. A.P. Newbery, B. Cantor, R.M. Jordan, and A.R.E. Singer: *J. Mater. Synthesis Processing,* 1996, vol. 4 pp. 1-13.